Research Article | Vol. 27, No. 2 | 21 Jan 2019 | OPTICS EXPRESS 714
Optics EXPRESS

Fast channel estimation and equalization scheme for offset-QAM OFDM systems

JIAN ZHAO[1,*] AND PAUL TOWNSEND[2]

[1]South China University of Technology, Guangzhou, China
[2]Photonics Systems Group, Tyndall National Institute, Lee Maltings, Dyke Parade, Cork, Ireland
*zhaojian@scut.edu.cn

Abstract: We show that the orthogonality between signal and intrinsic imaginary interference (IMI) in offset quadrature amplitude modulation (offset-QAM) orthogonal frequency division multiplexing (OFDM) can still be maintained under a certain condition even when the timing slots of different subcarriers are misaligned. We show that the phase and velocity differences over subcarriers induced by fiber dispersion satisfy this condition. Based on this, we propose a fast channel estimation and equalization scheme without prior channel information including coarse dispersion. We investigate the proposed scheme in a 40-Gbit/s offset-16QAM OFDM experiment and 240-Gbit/s polarization-division-multiplexed offset-16QAM OFDM simulations, both over 1200-km single-mode fiber. It is shown that the proposed scheme gives better performance, reduced overhead for the training sequence, and/or lower complexity than other schemes. We also compare offset-QAM OFDM with the proposed scheme and conventional OFDM, and show that in addition to the elimination of cyclic prefix overhead, offset-QAM OFDM gives better performance and longer transmission reach for a moderate/small number of subcarriers.

1. Introduction

Offset quadrature amplitude modulation (offset-QAM) orthogonal frequency division multiplexing (OFDM) has exhibited advantages in coherent super-channels, uplinks in passive optical networks, long-haul transmission, direct-detection systems, and radio-over-fiber systems [1–6]. In offset-QAM OFDM, the quadrature tributary of each subcarrier is delayed by half a symbol period with respect to the in-phase tributary of that subcarrier. For each tributary, crosstalk from adjacent subcarriers exists but is controlled to have $\pi/2$ phase difference from the desirable signal so that the signal can still be recovered without distortion. This crosstalk is called intrinsic imaginary interference (IMI). However, the responses of optical/electronic devices and fiber channels can break the orthogonality between IMI and the signal. In the literature, great efforts have been taken to investigate channel estimation and equalization schemes specific to offset-QAM OFDM [7–16]. In [7], four methods, including a specially designed training sequence and modified least-mean-square algorithm, were proposed to improve the system performance. These methods can precisely estimate the phase shifts in the response of opto-electronic devices. They also work well when the channel delay is small with respect to the OFDM symbol period. The interference approximation method (IAM), first proposed in wireless communications, was also migrated to optical offset-QAM OFDM [8–10]. This method assumes prior knowledge of IMI and uses this information to design the preamble to enhance the estimation performance. In [11], the IMI was adaptively estimated and compensated by multi-tap equalizers. However, these methods are only suitable in cases where the distortion on each subcarrier is negligible and the maximal delay difference between subcarriers is small with respect to the symbol period.

For high-speed optical systems with long transmission distances (100s-1000s km), the delay difference between subcarriers at the highest and lowest frequencies can be large. Dispersion not only results in different phases and timing delays for different subcarriers but

#342646 https://doi.org/10.1364/OE.27.000714
Journal © 2019 Received 17 Aug 2018; revised 1 Dec 2018; accepted 4 Dec 2018; published 9 Jan 2019

Optics EXPRESS

also distorts the pulse shape of each subcarrier. This effect is more severe when the number of subcarriers is small. In [12,13], multiple filter banks were used to decode all subcarriers simultaneously. However, this approach involves a tradeoff between performance and complexity. In addition, as will be shown in this paper, it cannot compensate the distortion on the pulse of each subcarrier. In [13–15], time-domain or frequency-domain filters were applied to equalize the channel on a subcarrier-by-subcarrier basis. However, they assume an ideally known channel response or require a long training sequence for channel estimation.

Although various channel estimation and equalization methods have been investigated in optical offset-QAM OFDM, the mechanism of IMI in the fiber channel has not been elucidated. To be specific, conventional offset-QAM OFDM assumes that the pulses of all subcarriers are aligned in time and there is a $\pi/2$ phase difference between adjacent subcarriers. It is well known that different subcarriers are no longer aligned in time after transmission and also the phase difference between adjacent subcarriers is not $\pi/2$. Therefore, it is desirable to know if IMI is still orthogonal to the signal in this case.

In this paper, we show that the orthogonality of offset-QAM OFDM can be maintained even when any subcarrier has any time delay, provided that the phase difference between that subcarrier and its adjacent subcarriers is equal to a value determined by their timing difference. It is also shown that dispersion-induced phase shift and timing delay satisfy this condition. Therefore, the IMI at the correct sampling phase of any particular subcarrier can still be orthogonal to the signal after transmission although its adjacent subcarriers do not have synchronized timing and $\pi/2$ phase difference. The distortion on the pulse of each subcarrier can also be compensated by updating the pulse shaping filter based on the sampling phase information. We propose a simple and fast channel estimation and equalization scheme without prior channel information including coarse dispersion. The scheme is applicable for both short and long distances as well as different numbers of subcarriers, even in cases where the channel delay exceeds the OFDM symbol period and the distortion on the pulse of each subcarrier is not negligible. We investigate the proposed scheme in a 40-Gbit/s offset-16QAM OFDM experiment and 240-Gbit/s polarization-division-multiplexed (PDM) offset-16QAM OFDM simulations, both over 1200-km single-mode fiber (SMF). It is shown that the proposed scheme gives better performance, reduced overhead for the training sequence, and/or lower complexity than multiple filter banks [12,13], multi-tap equalization [11], and subcarrier-by-subcarrier equalization [13–15]. We also compare offset-QAM OFDM with the proposed scheme and conventional OFDM, and show that in addition to the elimination of cyclic prefix (CP) overhead, offset-QAM OFDM can achieve better performance and longer transmission reach for a moderate/small number of subcarriers.

2. Principle

2.1 Orthogonality in the presence of timing misalignment between subcarriers

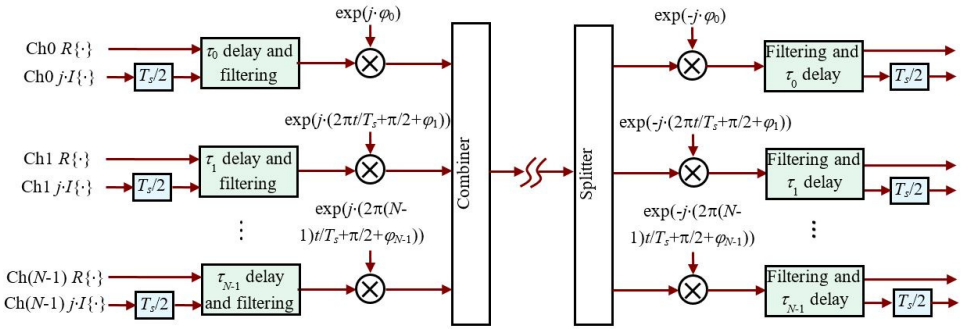

Fig. 1. Principle of offset-QAM OFDM with timing misalignment between subcarriers. T_s is the OFDM symbol period and is equal to $T{\cdot}N$. In the conventional system, $\tau_n = 0$ and $\varphi_n = 0$.

Optics EXPRESS

We firstly present the orthogonality condition when the timing slots of different subcarriers are not aligned, as shown in Fig. 1. This derived principle can be used to generate a generalized offset-QAM OFDM signal without the limitation of aligned time slots between subcarriers. In this paper, we will show that dispersion-induced phase and velocity differences over subcarriers satisfy this condition so that the orthogonality can still be maintained after transmission. Assuming that $a_{i,n}$ and $s(i\cdot N + k)$ are the n^{th} subcarrier data in the frequency domain and the k^{th} sample in the i^{th} offset-QAM OFDM symbol, $s(i\cdot N + k)$ is derived as:

$$\begin{aligned} s(i\cdot N+k) &= s^{real}(i\cdot N+k) + j\cdot s^{imag}(i\cdot N+k) \\ &= \sum_{p=-\infty}^{+\infty}\sum_{n=-N/2+1}^{N/2} a_{p,n}^{real}\exp(j\pi n/2 + j\varphi_n)\cdot\exp(2\pi jkn/N)\cdot h_{filter}(i\cdot N+k-p\cdot N-\tau_n/T) \\ &+ \sum_{p=-\infty}^{+\infty}\sum_{n=-N/2+1}^{N/2} a_{p,n}^{imag}\exp(j\pi(n+1)/2 + j\varphi_n)\cdot\exp(2\pi jkn/N)\cdot h_{filter}(i\cdot N+k-N/2-p\cdot N-\tau_n/T) \end{aligned} \tag{1}$$

where $k = -N/2 + 1, -N/2 + 2 \ldots N/2$. In Eq. (1), $h_{filter}(\cdot)$ represents the impulse response of the pulse shaping filter. T is the time interval between samples and N is the number of subcarriers. It is readily known that the OFDM symbol period T_s is equal to $T\cdot N$. The quadrature tributary is delayed by half a symbol period, $N/2$, with respect to the in-phase tributary. In contrast to conventional offset-QAM OFDM, a delay τ_n and a phase φ_n, both dependent on the index of subcarrier n, are introduced in Eq. (1).

At the receiver, without the loss of generality, we only derive the demodulated in-phase tributary of the m^{th} subcarrier in the i^{th} OFDM symbol, $b_{i,m}^{real}$:

$$\begin{aligned} b_{i,m}^{real} &= real\{\exp(-j\pi m/2 - j\varphi_m) \\ &\cdot \sum_{k=-N/2+1}^{N/2}\sum_{q=-\infty}^{+\infty}\exp(-2\pi jk\cdot m/N)\cdot s(q\cdot N+k)\cdot h_{receiver\_filter}((i-q)\cdot N-k+\tau_m/T)\} \end{aligned} \tag{2}$$

where $h_{receiver\_filter}((i\text{-}q)\cdot N\text{-}k + \tau_m/T)$ is the impulse response of the receiver matched filter and is equal to $h_{filter}(q\cdot N + k\text{-}i\cdot N\text{-}\tau_m/T)$. We would like to highlight that in Eq. (2), τ_m is added in $h_{receiver\_filter}$, representing that the m^{th} subcarrier should be sampled at $i\cdot N + \tau_m/T$. After detailed derivation in the Appendix I, we find that $b_{i,m}^{real}$ can be recovered without crosstalk even when the timing slots of different subcarriers are misaligned, provided that:

$$\varphi_{m+1} - \varphi_m = i\cdot\pi - \frac{\pi\cdot(\tau_{m+1}+\tau_m)}{NT} \tag{3}$$

where i is an arbitrary integer. The recovered $b_{i,m}^{real}$ is:

$$b_{i,m}^{real} = a_{i,m}^{real}\cdot\sum_{k=-N/2+1}^{N/2}\sum_{q=-\infty}^{+\infty} h_{filter}^2(q\cdot N+k-i\cdot N-\tau_m/T) \tag{4}$$

Figure 2 gives an example with misaligned time slots between subcarriers. We use baseband representation to denote the m^{th} subcarrier. The $(m + 1)^{th}$ subcarrier is delayed by $3T_s/8$ with respect to the m^{th} subcarrier. By controlling the phase of the $(m + 1)^{th}$ subcarrier, zero crosstalk can still be obtained at the correct sampling point of the m^{th} subcarrier. Figure 3 illustrates the principle to achieve zero crosstalk. Mathematically, the crosstalk at the sampling point is the integration of a function that is equal to the multiplication of 1). The baseband pulse of the $(m + 1)^{th}$ subcarrier; 2). The demultiplexing filter for the m^{th} subcarrier;

Optics EXPRESS

and 3) the carrier of the $(m + 1)^{th}$ subcarrier. To obtain zero crosstalk, this function should be odd symmetric to get zero value after integration. Therefore, we have:

$$\varphi_{m+1} - \varphi_m = i \cdot \pi - \frac{2\pi}{NT} \cdot \frac{(\tau_{m+1} + \tau_m)}{2} = i \cdot \pi - \frac{\pi(\tau_{m+1} + \tau_m)}{NT} \tag{5}$$

where i is an arbitrary integer. This interpretation confirms the result in Eq. (3).

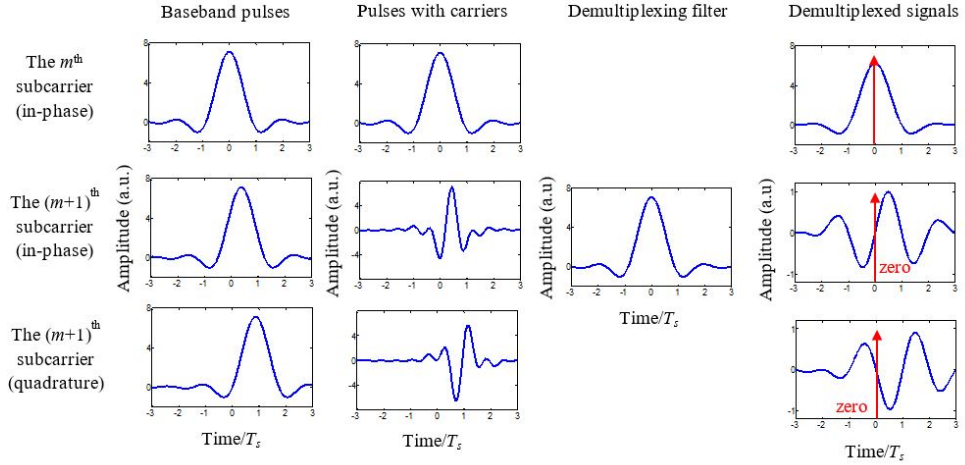

Fig. 2. An example to illustrate the crosstalk from the $(m + 1)^{th}$ subcarrier to the m^{th} subcarrier. In this example, the delay between the in-phase (or quadrature) tributary of the $(m + 1)^{th}$ subcarrier and the in-phase tributary of the m^{th} subcarrier is $3T_s/8$ (or $7T_s/8$).

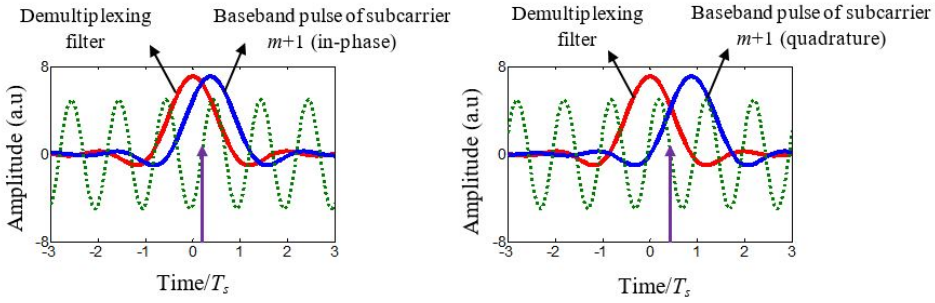

Fig. 3. An example to illustrate the condition to get zero crosstalk from the (a) in-phase and (b) quadrature tributaries of the $(m + 1)^{th}$ subcarrier, when there is a timing misalignment between subcarriers. The carrier phase in the figure should be controlled so that it is odd symmetric with respect to $(\tau_m + \tau_{m+1})/2$, where $\tau_m = 0$ and $\tau_{m+1} = 3T_s/8$ or $7T_s/8$ in (a) and (b), respectively.

Note that in the analysis, it is assumed that the sampling point of the m^{th} subcarrier is at τ_m; and there is no distortion on $h_{filter}(\cdot)$. In practice, it implies that in addition to the condition of Eq. (3), we should know the sampling phase of each subcarrier and compensate the distortion on $h_{filter}(\cdot)$ to maintain the orthogonality.

Equation (3) can be used to design a generalized offset-QAM OFDM system with an arbitrary delay profile over subcarriers. In addition, any transmission impairment that satisfies this condition would not break the orthogonality. In the next section, we will show that fiber dispersion satisfies Eq. (3), and so orthogonalty can be maintained although it is not required to have prior knowledge on the amount of dispersion.

Optics EXPRESS

2.2 Channel effect on offset-QAM OFDM

Fiber channel effects include those with a long memory length (such as coarse dispersion) and with a short memory length (such as residual dispersion, polarization mode dispersion, and responses from opto-electronic devices). In static fiber systems, the compensation of coarse dispersion, whose delay can be larger than the OFDM symbol period, is separated from adaptive equalization. This however increases the complexity and does not fully exploit the advantage of OFDM using one-tap equalizers. It is also not suitable to dynamical optical networks without the channel information. In addition, conventional OFDM systems assume a flat channel response on each subcarrier, which is not valid for high data rates per subcarrier. In this paper, we consider a general case: there is no prior channel information including coarse dispersion; the channel not only influences the phases and delays of subcarriers, but also distorts the pulse of each subcarrier. The channel frequency response at any frequency with the distance of $d/(TN)$ to the center frequency of the m^{th} subcarrier is:

$$\begin{aligned} H_c((m+d)/(TN)) &= H_p \cdot H_b((m+d)/(TN)) \cdot \exp(j \cdot \beta_2 L/2 \cdot (2\pi/(TN))^2 \cdot (m+d)^2) \\ &= \underbrace{H_p \cdot H_b((m+d)/(TN)) \cdot \exp(j\alpha d^2)}_{\text{effects with a short memeory length}} \cdot \underbrace{\exp(j \cdot (2\alpha md + \alpha m^2))}_{\text{effects with a long memory length}} \end{aligned} \quad (6)$$

where $H_c(\cdot)$ is the channel frequency response. H_p is the phase noise. $\beta_2 L$ is the accumulated dispersion. $\alpha = \beta_2 \cdot L \cdot (2\pi/(TN))^2/2$. $H_b(\cdot)$ represents the response of opto-electronic devices. In Eq. (6), we separate $H_c(\cdot)$ into two effects. Phase noise, channel responses from devices, and the distortion on the pulse of each subcarrier are those with a short memory length. In fact, the phase noise only results in phase rotations while the distortion on the pulse of each subcarrier is negligible for a large number of subcarriers (~100s MBaud per subcarrier). However, this distortion should be considered as the number of subcarriers reduces (several GBaud per subcarrier). The second part is the effects with a long memory length. Dispersion results in different velocities and phases for different subcarriers. For example, for a 30-GBaud 16QAM signal with 128 subcarriers, the bandwidth and symbol period per subcarrier are ~234 MHz and ~4.23 ns, respectively. After 1200-km SMF, the channel delay from the effects with a short memory length is ~38.3 ps, which is negligible with respect to the symbol period. However, the delay difference between subcarriers at the highest and lowest frequencies is 4.9 ns, which is larger than the OFDM symbol period.

For the effects with a long memory length in Eq. (6), we may rewrite $\exp(j\cdot(2\alpha md + \alpha m^2))$ as $\exp(2\pi j\cdot\alpha mNT/\pi\cdot d/(NT) + j\alpha m^2)$. Therefore, the timing delay and phase shift of the m^{th} subcarrier are $-\alpha mNT/\pi$ and αm^2, respectively, which satisfy Eq. (3):

$$\alpha(m+1)^2 - \alpha m^2 = \alpha(2m+1) = -\frac{\pi(-\alpha(m+1)NT/\pi - \alpha mNT/\pi)}{NT} \quad (7)$$

This implies that the orthogonality can still be maintained after transmission even when the timing slots of subcarriers are misaligned due to dispersion.

2.3 Proposed channel estimation and equalization scheme

Figure 4 shows the proposed scheme. This scheme can be applied to different transmission distances and different numbers of subcarriers, even in the cases where the channel delay exceeds the OFDM symbol period and the distortion on the pulse of each subcarrier is not negligible. The transmitter can be either conventional offset-QAM OFDM with synchronized timing or that in Fig. 1 with timing misalignment between subcarriers. In the former case, efficient discrete Fourier transform (DFT) can be used for multiplexing. The transmitted signal consists of a training sequence similar to M-LS-2 in [7]. At the receiver, after conversion to baseband, the training sequence of each subcarrier is extracted. Assuming that

Optics EXPRESS

$r_{training,m}(i\cdot N+k)$ is the k^{th} sample in the i^{th} OFDM training symbol for the m^{th} subcarrier. After derivations in Appendix II, the sampling phase of the m^{th} subcarrier is estimated as:

$$\tau_m / T = N \cdot (Angle(R_{training,m}(N-1)) - Angle(R_{training,m}(1))) / (4\pi) \quad (8)$$

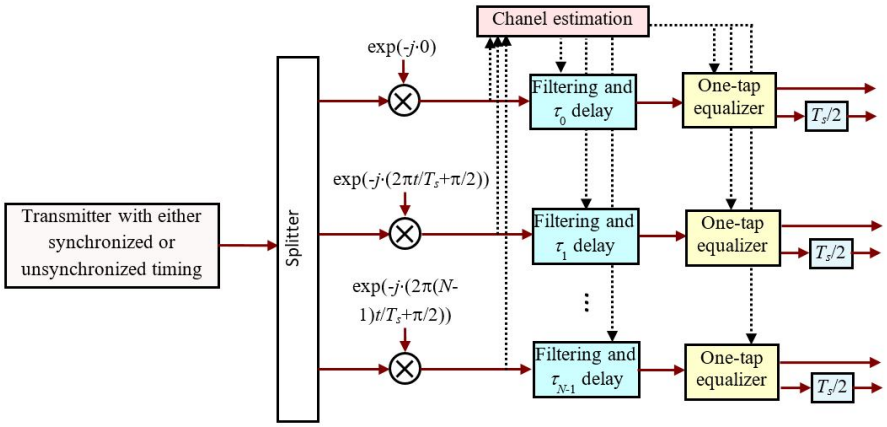

Fig. 4. Principle of the proposed channel estimation and equalization scheme.

where $Angle(\cdot)$ extracts the phase and $R_{training,m}(n)$ is:

$$R_{training,m}(n) = F_{k,n}\{\sum_{i=-N_t/2+1}^{N_t/2} \left| r_{training,m}(i\cdot N+k) \right|^2\} \qquad k = -N/2+1 \ldots N/2 \quad (9)$$

where $F_{k,n}\{\cdot\}$ is the Fourier transform, with k and n being the arguments of the functions before and after the Fourier transform respectively. N_t is the number of training symbols. As shown later, ~10 training symbols are sufficient to achieve near-optimal performance. This is much smaller than that required in other schemes. The estimation of τ_m is independent of the phase of $r_{training,m}(i\cdot N+k)$, so that this process can be conducted before phase recovery. Note that the estimated τ_m is in the range of $[-N/2+1\ N/2]$. For long transmission distances where the maximal delay difference of subcarriers (e.g. that between the highest and lowest frequencies) are larger than the OFDM symbol period, τ_m should be unfolded by adding N or $-N$. Because $\tau_m = -\alpha mNT/\pi$ and is linearly increasing/decreasing with m, this unfolding can be realized by observing τ_{m-1}, τ_{m-2} and so on. If the timing slots of subcarriers are not aligned at the transmitter, τ_m should be firstly modified according to the transmitter design before the unfolding. Finally, the estimated τ_m is distorted by noise. Therefore, we use first-order polynomial curve fitting to estimate α under $\tau_m = -\alpha mNT/\pi$, which in turn improves the estimation accuracy. The value obtained after the curve fitting is denoted as $\tau_{m,\text{improved}}$.

After $\tau_{m,\text{improved}}$ is recovered, each subcarrier is sampled at the correct sampling phase. Given the analysis in Subsection 2.1, dispersion-induced timing misalignment does not break the orthogonality. For the effects with a short memory length, the phase noise H_p can be compensated using various phase compensation algorithms [17,18]. In this paper, we use a pilot tone around DC to remove the phase noise. Re-using the training sequence for the estimation of τ_m can readily compensate $H_b(\cdot)$ [7]. Finally, $\exp(j\alpha d^2)$ represents the distortion on the pulse of each subcarrier. This effect is negligible for a large number of subcarriers but should be considered as the number of subcarriers reduces. Because α can be estimated from τ_m, we update the pulse shaping filter at the receiver to equalize the effect of $\exp(j\alpha d^2)$:

$$h_{receiver\_filter}(k) = h_{filter\_d}{}^{*}(-k) \quad (10)$$

$$h_{filter\_d}(k) = h_{filter}(k) \otimes F_{n,k}{}^{-1}\{\exp(j\alpha n^2)\} \quad (11)$$

Optics EXPRESS

where k is from -∞ to + ∞ and $F_{n,k}^{-1}\{\cdot\}$ is the inverse Fourier transform. After updating the pulse shaping filter, one-tap equalizers are used to compensate residual channel effects.

The complexity of the proposed scheme is only at the training stage, where the training sequence is used to find out the sampling phase, update the pulse shaping filter, and decide the coefficients of one-tap equalizers. As shown later, the required number of training symbols is much smaller than other schemes. After the estimation stage, the complexity of the equalization is the same as that in the conventional system. This is in contrast to other schemes such as multiple filter banks, multi-tap equalization, and subcarrier-by-subcarrier equalization, where additional complexity is required at the equalization stage.

3. Experimental setup and results

3.1 Experimental setup

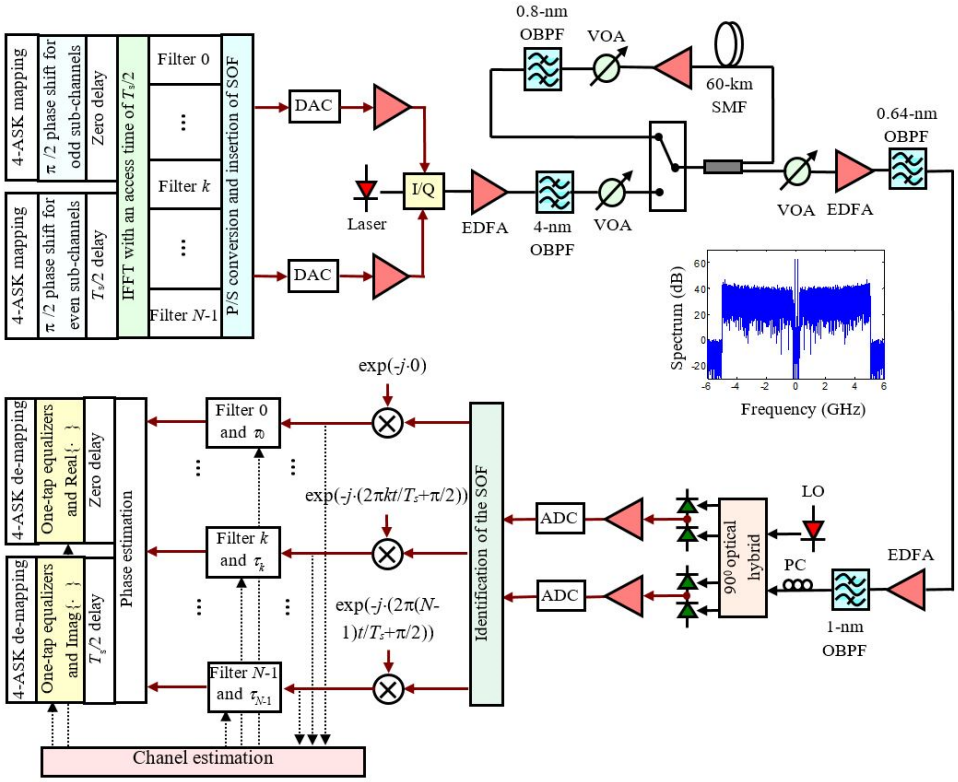

Fig. 5. Experimental setup

In this section, we reported the experimental results to illustrate the advantage of the proposed scheme. Figure 5 shows the experimental setup. The transmitter used DFT-based multiplexing for offset-QAM OFDM. The IFFT and FFT used 128 points, of which 102 subcarriers were used for 16QAM data modulation. The six subcarriers in the zero-frequency region were not modulated, allowing for AC-coupled amplifiers and insertion of pilot tones for phase estimation. The twenty subcarriers at the high frequencies were zero-padded to avoid aliasing. The pulse shaping filter created a square-root-raised-cosine (SRRC) function with a roll-off factor of 0.5. The OFDM sequence began with a start-of-frame (SOF) symbol. The training sequence for channel estimation was designed according to the principle in [7]. The inset of Fig. 5 shows the spectrum of the offset-QAM OFDM signal. The generated signal was clipped with 11-dB peak-to-average power ratio (PAPR) before downloaded to an arbitrary waveform generator with 12-GS/s digital-to-analogue converters (DACs).

Optics EXPRESS

The electrical OFDM signal was fed into an optical I/Q modulator with a peak-to-peak driving swing of $0.5V_{\pi}$. The generated optical signal was amplified by an erbium doped fiber amplifier (EDFA), filtered by a 4-nm optical band-pass filter (OBPF), and transmitted over a recirculating loop comprising 60-km SMF with 14-dB fiber loss. The noise figure of the EDFA was 6 dB and another 0.8-nm OBPF was used in the loop to suppress the amplified spontaneous emission noise. The launch power per span was around –9 dBm. At the receiver, the optical signal was detected with a pre-amplified coherent receiver. A variable optical attenuator (VOA) was used to vary the optical signal-to-noise ratio (OSNR) for bit error rate (BER) measurements. The pre-amplifier was followed by an OBPF with a 3-dB bandwidth of 0.64 nm, a second EDFA, and another OBPF with a 3-dB bandwidth of 1 nm. A polarization controller (PC) was used to align the polarization of the filtered OFDM signal before entering the signal path of a 90° optical hybrid. The optical outputs of the hybrid were connected to two balanced photodiodes with 40-GHz 3-dB bandwidths, amplified by 40-GHz electrical amplifiers, and captured using a 50-GS/s real-time oscilloscope. The received signal was re-sampled and equalized using the principle in Section 2.

We also implemented three other equalization/decoding schemes for comparison: 1. multiple filter banks (MFB) scheme which employed multiple decoding blocks with each consisting of a DFT and one-tap equalizers [12]; 2. multi-tap equalizers (MTE) that used one DFT for demultiplexing and multi-tap equalizers to compensate the IMI between subcarriers [11,13]. The number of real taps was 15 to include the inter-symbol interference (ISI) from adjacent symbols and inter-carrier interference (ICI) from adjacent subcarriers; 3. subcarrier-by-subcarrier equalizers (SSE) that applied a multi-tap equalizer for each subcarrier after the pulse shaping filter [13–15]. In MTE and SSE, least-mean-square algorithm was used to acquire the coefficients and the convergence parameter was optimized.

3.2 Experimental results

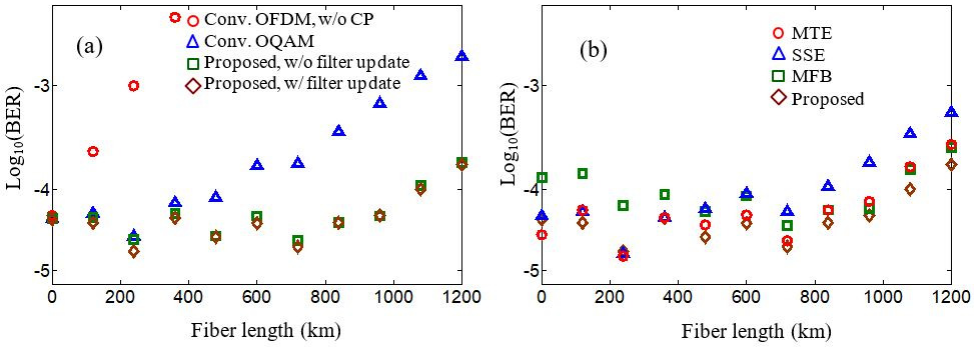

Fig. 6. (a) BER versus fiber length for conventional OFDM, conventional offset-QAM OFDM, and offset-QAM OFDM with the proposed scheme. (b) BER versus fiber length for offset-QAM OFDM with different equalization schemes. The numbers of training symbols for MTE, SSE, MFB, and the proposed scheme are 160, 64, 64, and 32, respectively.

Figure 6(a) shows the BER versus fiber length for conventional OFDM, conventional offset-QAM OFDM and offset-QAM OFDM with the proposed scheme. The OSNR values for 0, 120, 240, 360, 480, 600, 720, 840, 960, 1080, and 1200 km are 16, 15.5, 16.7 16.1, 16.7, 16.2 16.8, 16.7, 16.3, 15.9, and 15.6 dB, respectively. CP is not applied in any of the cases. The figure shows that the conventional OFDM cannot support 400-km transmission at the BER of 10^{-3}. Offset-QAM OFDM greatly improves the performance. However, the BER still increases for distances longer than 500 km. By using the proposed scheme, the orthogonality between the IMI and the signal can be maintained for each subcarrier, even when the time slots of different subcarriers are misaligned after transmission. Residual channel effects with a short memory length can be compensated via one-tap equalizers. Therefore, the BER is

Optics EXPRESS

reduced from ~10^{-3} to ~10^{-4} at 15.6-dB OSNR and 1200 km. Note that at 10 GBaud with 128 subcarriers and 1200-km transmission distance, the distortion on the pulse of each subcarrier is negligible. Therefore, there is no performance degradation even when we do not update the pulse shaping filter via Eqs. (10)-(11).

Figure 6(b) compares the performance of different equalization schemes. In this figure, MFB uses two DFTs and the delay between these DFTs is optimized at 1200 km. The numbers of training symbols for MTE, SSE, MFB, and the proposed scheme are 160, 64, 64, and 32, respectively. It can be seen that the proposed scheme gives the best performance regardless of the fiber length. Multi-tap equalizers can achieve similar performance as the proposed scheme, but as will be shown later, it requires a longer training sequence and has a limited transmission reach for higher-speed systems. SSE exhibits a performance penalty for distances longer than 600 km. Finally, MFB can achieve similar performance as the proposed scheme at long distances but shows a performance penalty at short distances. This is because the delay between DFTs in MFB is optimized at 1200 km.

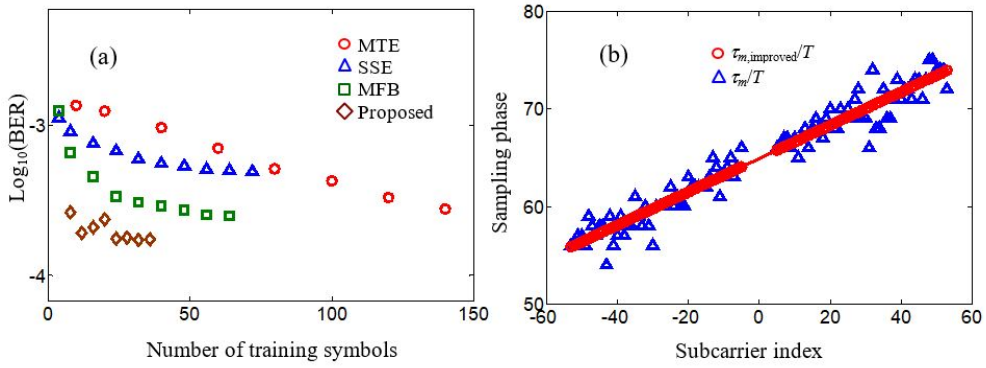

Fig. 7. (a) BER versus the number of training symbols for different equalization schemes at 1200 km. (b) Estimated τ_m/T and $\tau_{m,\text{improved}}/T$ for the proposed scheme at 1200 km.

Figure 7(a) depicts the performance versus the number of training symbols for different schemes at 1200 km. In the figure, MFB uses two DFTs and the delay between these DFTs is optimized at 1200 km. It is seen that MTE requires the largest number of training symbols. However, its performance can approach to that of the proposed scheme as the number of training symbols increases. SSE requires a smaller number of training symbols. However, the saturated performance is poorer than other schemes. For the MFB scheme, ~40 training symbols can achieve near-optimal performance. The proposed scheme requires the shortest training sequence and ~10 training symbols can achieve the best performance. Figure 7(b) shows the estimated τ_m/T and $\tau_{m,\text{improved}}/T$ for the proposed scheme. τ_m is estimated from Eq. (8) and is influenced by the noise. Because dispersion-induced timing delay has a linear profile over frequency or subcarriers (= $-\alpha mTN/\pi$ as discussed in Section 2.2), $\tau_{m,\text{improved}}$ can be obtained from the fitting curve of τ_m to enhance the estimation accuracy.

For the MFB scheme in Figs. 6-7, two DFTs with the delay optimized at 1200 km are used. It is shown that there is a penalty at short distances. In addition, we may not know the fiber length and optimize this delay in practice. Figure 8(a) shows the BER versus the delay for 2 and 4 DFTs. Figure 8(b) depicts their BER versus the fiber length. From the figures, we can see that the BER is less sensitive to the delay and the fiber length by using a larger number of DFTs. This can be understood as follows: different subcarriers spread in time due to dispersion. Multiple DFTs are used so that each subcarrier would choose the suitable DFT, whose timing is nearest to the delay of that subcarrier, for decoding. Clearly, a larger number of DFTs would give a higher resolution so that the performance is less sensitive to the fiber length. In addition, for longer transmission distances, the delay difference between subcarriers

Optics EXPRESS

at the highest and lowest frequencies can exceed the OFDM symbol period. Therefore, without the channel information, the optimal solution is to place K DFTs with $N(i\text{-}1)/K$ delay for each DFT, where $i = 1 \ldots K$, to cover all possible delays of subcarriers. This design will be used in the next section. Note that a larger number of DFTs requires higher complexity, and so there is a tradeoff between the complexity and penalty.

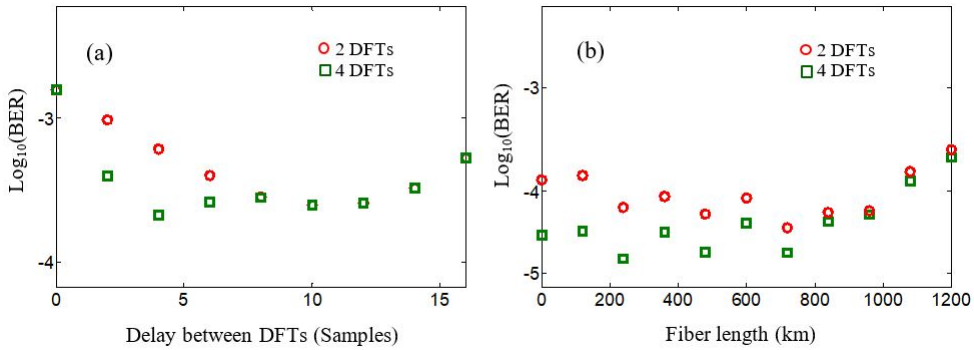

Fig. 8. (a) BER versus the delay between DFTs in the MFB scheme at 1200 km. (b) BER versus fiber length for the MFB scheme with different numbers of DFTs.

4. Simulation setup and results

The advantages of the proposed scheme have not been fully explored via the experiment, especially for higher baud rates. In this section, we simulated 240-Gb/s PDM offset-16QAM OFDM. The sampling rate of the DACs was 40 GS/s. The number of subcarriers varied and the number of zero-padded subcarriers was controlled such that the signal rate was 240 Gb/s. The FIR filters created a SRRC pulse shape with a roll-off factor of 0.5. After DACs, low-pass filters with 22-GHz bandwidth were used to remove the aliasing. The peak to average power ratio of the electrical signal was 10 dB. The linewidth of the transmitter laser and the local oscillator was 100 kHz. The signals of two polarizations were modulated, combined, and launched into fiber links. The dispersion parameter, nonlinear coefficient, and loss of the fibers were –21.7 ps^2/km, 1.5/km/W, and 0.22 dB, respectively. The noise figure of the EDFAs in the fiber links was 5 dB. At the receiver, the signals were filtered by a 40-GHz optical filter and coherently detected. The bandwidth of the receiver frontend was 40 GHz and the sampling rate of the ADCs was 40 GS/s.

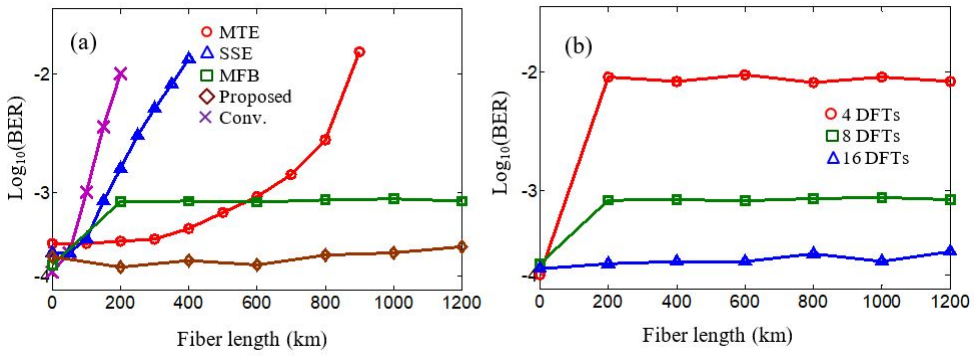

Fig. 9. (a) BER versus fiber length for different equalization schemes. The number of DFTs in the MFB scheme is 8. (b) BER versus fiber length for the MFB scheme with different number of DFTs. In both figures, fiber nonlinearity is not included and the OSNR is 22 dB.

Optics EXPRESS

We firstly neglect the fiber nonlinearity. Figure 9(a) shows the performance of different equalization schemes when the number of subcarriers is 128. The number of training symbols for MTE, SSE, MFB, and the proposed scheme are 160, 64, 64, 32 respectively. The baud rate is ~3 times that used in the experiment. The MFB scheme uses 8 DFTs with $N(i\text{-}1)/8$ delay for the i^{th} DFT. It is seen that similar to the experiment, SSE is unable to acquire the channel information effectively. In the literature, either ideal channel information is assumed or a large number (1000s) of training symbols is required for this scheme [13–15]. MTE can improve the performance but can only support transmissions over 100s km. It is because this scheme is only effective in cases where the channel delay is small with respect to the OFDM symbol period. Note that the number of taps in MTE is 15. A larger number of taps may improve the performance but increases the complexity. MFB can achieve stable performance over all fiber lengths. However, it exhibits a penalty due to the limited resolution. For 8 DFTs, the maximal timing misalignment between a subcarrier and its decoding DFT is $T_s/16$. In contrast, the proposed scheme maintains low BERs for all investigated distances, clearly showing the performance advantage. Figure 9(b) shows the performance of MFB for different DFTs. When 4 DFTs are used, the maximal timing misalignment between a subcarrier and its decoding DFT is $T_s/8$. Therefore, a higher penalty is observed. The use of 16 DFTs can eliminate this penalty but significantly increases the complexity.

Figure 9 is based on 128 subcarriers where the baud rate of each subcarrier is in the scale of 100s MBaud. In this case, the distortion on the pulse of each subcarrier is negligible. Figure 10(a) depicts the BER of the MFB scheme and the proposed scheme under different numbers of subcarriers. It is seen that in addition to the penalty due to the limited resolution of 8 DFTs, the performance of the MFB scheme degrades significantly as the number of subcarriers reduces. Additional simulations show that this distortion also exists when 16 DFTs are used. It is because the baud rate of each subcarrier increases for a smaller number of subcarriers, e.g. ~2.5 GBaud for 16 subcarriers. Therefore, dispersion-induced distortion on the pulse of each subcarrier is not negligible and the MFB scheme cannot compensate this effect. On the other hand, the proposed scheme updates the pulse shaping filter via Eq. (10), and readily compensates this distortion. Figure 10(b) shows the BER of the proposed scheme without and with updated pulse shaping filter using Eq. (10). It is confirmed that the performance is significantly degraded when the filters are not updated.

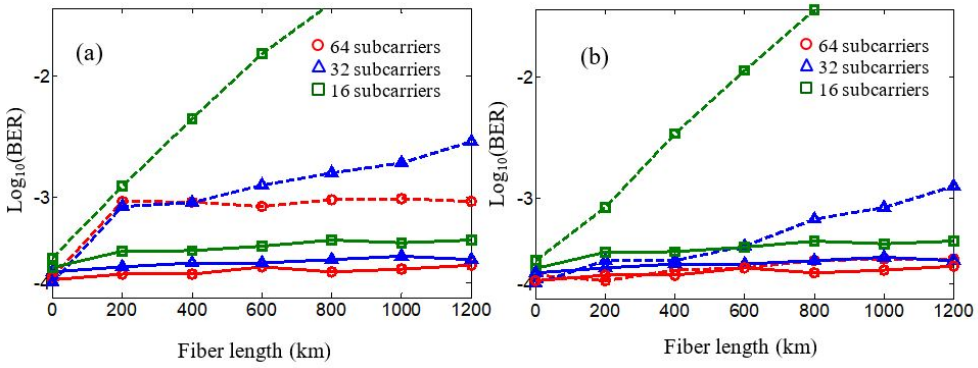

Fig. 10. (a) BER versus fiber length for the MFB (dashed) and the proposed (solid) schemes under different number of subcarriers. The number of DFTs in the MFB scheme is 8. (b) BER versus fiber length for the proposed scheme without (dashed) and with (solid) updated pulse shaping filter. In both figures, fiber nonlinearity is not included and the OSNR is 22 dB.

The proposed scheme can compensate the distortion on the pulse of each subcarrier because dispersion (including coarse dispersion) can be estimated to update the pulse shaping filter. Figure 11(a) shows the estimation error versus the actual dispersion when the sampling phase of the ADC is zero and 6.25 ps. It is seen that the estimation error is within ± 50 ps/nm

Optics EXPRESS

for the dispersion as large as ~2 × 10^4 ps/nm (corresponding to 1200 km) for both cases. Figure 11(b) shows the BER versus the sampling phase of the ADC when the root mean square (RMS) of the ADC timing jitter is 0 ps, 0.25 ps, 0.5 ps and 1 ps. Note that the sampling phase of the ADC is different from that in Eq. (8). The ADC has a sampling rate of 40 GS/s and its sampling phase is within the sample interval T. On the other hand, the pulse width of a subcarrier is in the scale of T_s (800 ps for 32 subcarriers) and Eq. (8) derives which sample is at the pulse center. It is clear from the figure that the performance of the proposed scheme is not sensitive to the sampling phase of the ADC. It is because a timing delay within the sample interval T is small with respect to the pulse width of a subcarrier (~$T_s = NT$) while that beyond T can be well estimated by Eq. (8). On the other hand, timing jitter influences the estimation accuracy of Eq. (8) and the performance degrades as the timing jitter increases. However, the penalty is small when the RMS is <0.5 ps. This is within the specification of commercial ADCs (commonly < 200-fs RMS). Therefore, timing jitter would not have significant influence on the performance of the proposed scheme in practice.

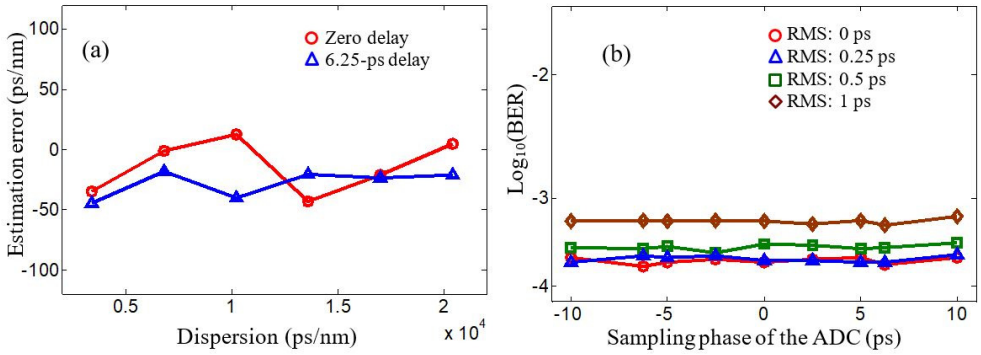

Fig. 11. (a) Estimation error versus actual fiber dispersion when the sampling clock of the ADC has a timing delay of 0 (circles) and 6.25 ps (triangles). (b) BER versus the sampling phase of the ADC under different timing jitters. Fiber length is 1200 km. In both figures, the number of subcarriers is 32 and the OSNR is 22 dB.

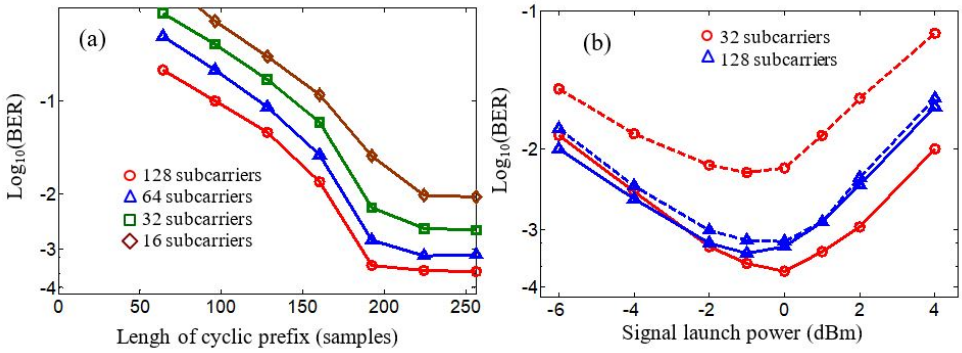

Fig. 12. (a) BER versus the CP length for conventional OFDM at 1200 km and 22-dB OSNR. (b) BER versus signal launch power for conventional OFDM (dashed) and offset-QAM OFDM with the proposed scheme (solid) at 1200 km. Fiber nonlinearity is included and the CP length for conventional OFDM is 224.

Next, we compare offset-QAM OFDM with the proposed scheme and conventional OFDM. It is well known that offset-QAM OFDM avoids the use of CP and increases the net spectral efficiency. In order to show this advantage, Fig. 12(a) depicts the performance versus the length of CP for conventional OFDM. It is seen that for all numbers of subcarriers, the length of CP should be larger than 224 to obtain the optimal performance. This implies that

Optics EXPRESS

the net spectral efficiency of conventional OFDM reduces to 6.7%, 12.5%, 22.2% and 36.4% of that in offset-QAM OFDM for 16, 32, 64, and 128 subcarriers, respectively. In addition, it is seen that the saturated performance of conventional OFDM degrades as the number of subcarriers reduces. This is because conventional OFDM cannot compensate the distortion on the pulse of each subcarrier. Therefore, the advantage of offset-QAM OFDM is more prominent for higher speed, longer distance, and a smaller number of subcarriers. A smaller number of subcarriers also results in a higher tolerance to the fiber nonlinearity. In Fig. 12(b), it is shown that the use of 32 subcarriers improves the performance in offset-QAM OFDM, especially in the nonlinear region. In contrast, conventional OFDM exhibits poorer performance by using 32 subcarriers, due to the reason described in Fig. 12(a).

5. Summary

In this paper, we have shown that the orthogonality of offset-QAM OFDM can be maintained even when any subcarrier has any time delay, provided that the phase difference between that subcarrier and its adjacent subcarriers is controlled. It is also shown that dispersion-induced phase shift and timing delay satisfy this condition. Therefore, the IMI at the correct sampling phase of any subcarrier can still be orthogonal to the signal after transmission although its adjacent subcarriers do not have synchronized timing and $\pi/2$ phase difference. The distortion on the pulse of each subcarrier can also be compensated by updating the pulse shaping filter based on the sampling phase information. We propose a fast channel estimation and equalization scheme without prior channel information including coarse dispersion. The scheme can be applied to both short and long distances as well as different numbers of subcarriers, even in cases where the channel delay exceeds the OFDM symbol period and the distortion on the pulse of each subcarrier is not negligible. We have investigated the proposed scheme in a 40-Gbit/s offset-16QAM OFDM experiment and 240-Gbit/s PDM offset-16QAM OFDM simulations, both over 1200-km SMF. It is shown that the proposed scheme gives better performance, reduced overhead for the training sequence, and/or lower complexity than the MFB, MTE and SSE schemes. We have also compared offset-QAM OFDM with the proposed scheme and conventional OFDM. It is shown that in addition to the elimination of the CP overhead, offset-QAM OFDM can achieve better performance and longer transmission reach for a moderate/small number of subcarriers.

Appendix I

We will derive Eq. (3) in this Appendix. By combing Eqs. (1) and (2), we can obtain:

Optics EXPRESS

$$
\begin{aligned}
b_{i,m}^{real} &= a_{i,m}^{real} \cdot \sum_{k=-N/2+1}^{N/2} \sum_{q=-\infty}^{+\infty} h_{filter}^2(q \cdot N + k - i \cdot N - \tau_m / T) \\
&+ real\{ \sum_{p=-\infty}^{+\infty} \sum_{k=-N/2+1}^{N/2} \sum_{q=-\infty}^{+\infty} a_{p,m+1}^{real} \cdot \exp(j \cdot (2\pi k / N + \pi / 2 + \varphi_{m+1} - \varphi_m)) \\
&\cdot h_{filter}(q \cdot N + k - p \cdot N - \tau_{m+1} / T) \cdot h_{filter}(q \cdot N + k - i \cdot N - \tau_m / T)\} \\
&+ real\{ \sum_{p=-\infty}^{+\infty} \sum_{k=-N/2+1}^{N/2} \sum_{q=-\infty}^{+\infty} a_{p,m+1}^{imag} \cdot \exp(j \cdot (2\pi k / N + \pi + \varphi_{m+1} - \varphi_m)) \\
&\cdot h_{filter}(q \cdot N + k - N/2 - p \cdot N - \tau_{m+1} / T) \cdot h_{filter}(q \cdot N + k - i \cdot N - \tau_m / T)\} \\
&+ real\{ \sum_{p=-\infty}^{+\infty} \sum_{k=-N/2+1}^{N/2} \sum_{q=-\infty}^{+\infty} a_{p,m-1}^{real} \cdot \exp(j \cdot (-2\pi k / N - \pi / 2 + \varphi_{m-1} - \varphi_m)) \\
&\cdot h_{filter}(q \cdot N + k - p \cdot N - \tau_{m-1} / T_{filter}(q \cdot N + k - i \cdot N - \tau_m / T)\} \\
&+ real\{ \sum_{p=-\infty}^{+\infty} \sum_{k=-N/2+1}^{N/2} \sum_{q=-\infty}^{+\infty} a_{p,m-1}^{imag} \cdot \exp(j \cdot (-2\pi k / N + \varphi_{m-1} - \varphi_m)) \\
&\cdot h_{filter}(q \cdot N + k - N/2 - p \cdot N - \tau_{m-1} / T) \cdot h_{filter}(q \cdot N + k - i \cdot N - \tau_m / T)\}
\end{aligned} \tag{12}
$$

Here, we use the property that $h_{filter}(\cdot)$ satisfies the inter-symbol interference free criterion, and the inter-carrier interference on the m^{th} subcarrier is only from its adjacent subcarriers. The first term on the right-hand side of Eq. (12) is the desirable signal. The other four terms are the IMI from the in-phase and quadrature tributaries of adjacent subcarriers. To enable the orthogonality, we need to ensure that the terms in each $Real\{\cdot\}$ is an imaginary value. We take the second term on the right-hand side of Eq. (12) as an example. Because $a_{p,i}^{real}$ is real and $h_{filter}(q \cdot N + k - p \cdot N - \tau_{m+1} / T) \cdot h_{filter}(q \cdot N + k - i \cdot N - \tau_m / T)$ is an even function with respect to $(p + i) \cdot N/2 + (\tau_{m+1} + \tau_m)/2/T$. Therefore, $\cos(2\pi k/N + \pi/2 + \varphi_{m+1}-\varphi_m)$ should be an odd function with respect to $(p + i) \cdot N/2 + (\tau_{m+1} + \tau_m)/2/T$. That is, $2\pi((p + i) \cdot N/2 + (\tau_{m+1} + \tau_m)/2/T)/N + \varphi_{m+1}-\varphi_m$ should be equal to an integer of π. This gives Eq. (3). The other three terms on the right-hand side of Eq. (12) can be analyzed in a similar way.

Appendix II

We will derive Eqs. (8) and (9) in this Appendix. The training sequence is designed as in [7] so that there is no ICI between subcarriers. The received training signal for the m^{th} subcarrier after the demultiplexing, $r_{training,m}(i \cdot N+k)$, is represented as:

$$
r_{training,m}(i \cdot N + k) = \sum_{p=-\infty}^{+\infty} a_{training,p,m} \cdot h(i \cdot N + k - p \cdot N - \tau_m / T) \tag{13}
$$

where $a_{training,p,m}$ is the training data in the p^{th} symbol and at the m^{th} subcarrier. $h(\cdot)$ is the pulse shape after the demultiplexing and also includes the effects of phase noise and the response of opto-electronic devices. Because $a_{training,p,m}$ in different symbols are uncorrelated, we can get:

$$
E\{\left| r_{training,m}(i \cdot N + k) \right|^2\} \propto \sum_{p=-\infty}^{+\infty} \left| h(i \cdot N + k - p \cdot N - \tau_m / T) \right|^2 \tag{14}
$$

In practice, $E\{\cdot\}$ is realized by averaging a certain number of training symbols, as used in Eq. (9). The right hand side of Eq. (14) is a periodic function and its DFT is:

$$
R_{training,m}(n) = \exp(-j \cdot \frac{2\pi n}{N} \cdot \frac{\tau_m}{T}) \cdot F_{k,n}\{ \sum_{p=-\infty}^{+\infty} \left| h(i \cdot N + k - p \cdot N) \right|^2 \} \tag{15}
$$

Optics EXPRESS

Because $|h(\cdot)|^2$ is a symmetric function and the term $F_{k,n}\{\cdot\}$ is real, Eq. (8) can be obtained.

Funding

China "1000 Youth Talent Program"; Science Foundation Ireland (SFI) (12/IA/1270, 12/RC/2276, 15/CDA/3652).

References

1. J. Zhao and A. D. Ellis, "Offset-QAM based coherent WDM for spectral efficiency enhancement," Opt. Express **19**(15), 14617–14631 (2011).
2. A. Saljoghei, F. A. Gutierrez, P. Perry, D. Venkitesh, R. D. Koipillai, and L. P. Barry, "Experimental comparison of FBMC and OFDM for multiple access uplink PON," J. Lightwave Technol. **35**(9), 1595–1604 (2017).
3. J. Fickers, A. Ghazisaeidi, M. Salsi, G. Charlet, P. Emplit, and F. Horlin, "Multicarrier offset-QAM for long-haul coherent optical communications," J. Lightwave Technol. **32**(24), 4069–4076 (2014).
4. Z. Li, T. Jiang, H. Li, X. Zhang, C. Li, C. Li, R. Hu, M. Luo, X. Zhang, X. Xiao, Q. Yang, and S. Yu, "Experimental demonstration of 110-Gb/s unsynchronized band-multiplexed superchannel coherent optical OFDM/OQAM system," Opt. Express **21**(19), 21924–21931 (2013).
5. J. Zhao and C. K. Chan, "Adaptively loaded SP-offset-QAM OFDM for IM/DD communication systems," Opt. Express **25**(18), 21603–21618 (2017).
6. M. Xu, J. Zhang, F. Lu, J. Wang, L. Cheng, M. I. Khalil, D. Guidotti, and G. K. Chang, "Orthogonal multiband CAP modulation based on offset-QAM and advanced filter design in spectral efficient MMW RoF systems," J. Lightwave Technol. **35**(4), 997–1005 (2017).
7. J. Zhao, "Channel estimation in DFT-based offset-QAM OFDM systems," Opt. Express **22**(21), 25651–25662 (2014).
8. N.-Q. Nhan, P. Morel, S. Azou, M. Morvan, P. Gravey, and E. Pincemin, "Sparse preamble design for polarization division multiplexed CO-OFDM/OQAM channel estimation," J. Lightwave Technol. **36**(13), 2737–2745 (2018).
9. X. Fang, Y. Xu, Z. Chen, and F. Zhang, "Frequency-domain channel estimation for polarization-division multiplexed CO-OFDM/OQAM systems," J. Lightwave Technol. **33**(13), 2743–2750 (2015).
10. X. Fang, Y. Xu, Z. Chen, and F. Zhang, "Time-domain least square channel estimation for polarization-division multiplexed CO-OFDM/OQAM sysems," J. Lightwave Technol. **34**(3), 891–900 (2016).
11. Y. Yu, P. D. Townsend, and J. Zhao, "Equalization of dispersion-induced crosstalk in optical offset-QAM OFDM systems," IEEE Photonics Technol. Lett. **28**(7), 782–785 (2016).
12. J. Zhao and P. D. Townsend, "Dispersion tolerance enhancement using an improved offset-QAM OFDM scheme," Opt. Express **23**(13), 17638–17652 (2015).
13. F. Rottenberg, T.H. Nguyen, S.P. Gorza, F. Horlin, and J. Louveaux, "Advanced chromatic dispersion compensation in optical fiber FBMC-OQAM systems," IEEE Photon. J. **9**(6) 7204710 (2017).
14. T.-H. Nguyen, F. Rottenberg, S.-P. Gorza, J. Louveaux, and F. Horlin, "Efficient chromatic dispersion compensation and carrier phase tracking for optical fiber FBMC/OQAM systems," J. Lightwave Technol. **35**(14), 2909–2916 (2017).
15. Z. Zheng, F. Frey, P. W. Berenguer, and J. K. Fischer, "Low-complexity equalization scheme for multicarrier offet-QAM systems," IEEE Photonics Technol. Lett. **29**(23), 2075–2078 (2017).
16. D. Wang, L. Yuan, J. Lei, G. Wu, S. Li, R. Ding, and D. Wang, "Joint channel/frequency offset estimation and correction for coherent optical FBMC/OQAM system," Opt. Fiber Technol. **39**, 87–94 (2017).
17. H. Tang, S. Fu, H. Liu, M. Tang, P. Shum, and D. Liu, "Low-complexity carrier phase recovery based on constellation classification for M-ary offset-QAM signal," J. Lightwave Technol. **34**(4), 1133–1140 (2016).
18. T. H. Nguyen and C. Peucheret, "Kalman filtering for carrier phase recovery in optical offset-QAM Nyquist WDM systems," IEEE Photonics Technol. Lett. **29**(12), 1019–1022 (2017).